CHAPTER 4

Alternative Nonlinear Demand Estimation Methods for Probability-Based Seismic Assessment

Jalayer, F. and Cornell, C. A. (2003 a). Earthquake Spectra, (in preparation).

4.1 Abstract

Demand and capacity factored design (DCFD) is a probability-based LRFD-like format used for seismic reliability assessment of structures. This format makes use of the results of nonlinear dynamic analysis in order to make probabilistic statements about the seismic reliability of a structure. This chapter discusses alternative methods for designing a program of nonlinear analyses and for applying the results of dynamic analysis in the framework of this demand and capacity factored design format, particularly as it relates to displacement-based demand estimation. These alternative methods are demonstrated through a comprehensive case study of an older reinforced concrete frame structure in Los Angeles. The dynamic analyses are performed on a set of ground motion records selected from a catalog of California events recorded on stiff soil. The spectral acceleration at the first mode period has been chosen as the representative ground motion intensity measure for the analysis, although the proposed methods are general with respect to the choice of the intensity measure. The methods are classified into narrow-range and wide-range methods, based on the range of spectral acceleration and displacement values for which they provide demand estimations. Single-stripe analysis and cloud analysis are two narrow-range methods discussed in this chapter. Wide-range methods employ rather extensive analysis efforts in order to provide estimations of displacement-based demand over a wider range of spectral accelerations. Multiple-stripe analysis and incremental dynamic analysis are examples of wide range methods. This chapter briefly addresses how incremental dynamic analysis method can also be used for displacement-based collapse limit state (capacity) estimation. The estimated displacement demand and capacity are compared -in the framework of DCFD in order to check the safety of the structure for the limit state of collapse. The uncertainty in the estimation of median displacement demand due to limited sample size, i.e., number of records, is also discussed. The procedure stated here can be used in practical applications: they are fully consistent with, for example, the FEMA/SAC (see FEMA 350-352) Guidelines although they address only the aleatory component of the demand factor.

4.2 Keywords

Probability-based seismic assessment, reinforced concrete frame structures, displacement-based demand, displacement-based capacity, ground motion intensity measure, spectral acceleration, seismic hazard, randomness, uncertainty.

4.3 Introduction

This chapter discusses alternative methods for the estimation of nonlinear dynamic structural displacement demand in the context of probabilistic seismic assessment. Demand estimation is an essential part of the demand and capacity factored design format for seismic assessment of structures. It is presumed here that a set of nonlinear dynamic analyses will be employed in order to make this estimation. One of the objectives here is efficient demand estimation, namely, finding procedures that estimate demand with acceptable accuracy and with minimum amount of analysis effort. Most of these methods are based on a simplified closed-form expression for demand and capacity factored design developed in Chapter 3 (Equation 3-12), which in turn stems from a closed-form derivation of annual frequency of exceeding limit state capacity developed in Chapter 2 (Equation 2-38).

The following expression represents the collective efforts leading to the calculation of the annual frequency of exceeding a structural limit state capacity, λ_{LS} [1]:

$$\lambda_{LS} = \lambda[capacity < demand] = \sum_y \sum_x P[capacity < demand \mid demand = y] \cdot P[demand = y \mid S_a = x] \cdot \lambda[S_a = x] \qquad (4\text{-}1)$$

The first factor within the sum is the probability that the random capacity is less than some displacement value *y*, the second factor is the probability that the displacement demand value is equal to y for a ground motion intensity level (e.g., here the first mode spectral acceleration, S_a) equal to *x* and the last factor is the annual frequency that the spectral acceleration is equal to *x*.

[1] Note that in the earlier chapters in this thesis we used the notation $H(.)$ to refer to the annual frequency of exceedance, whereas, in this chapter and also the ones to follow we are going to use the notation $\lambda(.)$ instead.

The limit state probability is obtained by summing the product of these three factors over all the possible values of x and y. A corresponding integral representation will follow below.

Assessment of the three factors in the above integrand (Equation 4-1) can be classified into capacity assessment, demand assessment and hazard assessment categories, respectively. This chapter focuses on the techniques that are available for demand assessment, that is, the estimation of probability distribution of demand for a given spectral acceleration.

Several design and assessment formats have been developed based on various manifestations of the expression for annual frequency of exceeding the limit state capacity (Equation 4-1). The formats, as such, enable the designer to design new structures and also to assess the seismic performance of existing structures. One such format is the Demand and Capacity Factored Design (DCFD) format developed in the previous chapter, analogous to typical equations for Load and Resistance Factored Design (LRFD) specifications (see Galambos and Ravindra, 1978). This format is expressed in the form, $\phi R \geq \gamma L$, where the factors ϕ and γ are applied to nominal resistance, R, and load, L. The Demand and Capacity Factored Design (DCFD) Format is based on the following representation of the expression for annual frequency of exceeding the limit state capacity:

$$median\ capacity \times capacity\ factor \leq median\ demand \times demand\ factor \qquad (4-2)$$

Where the median demand is associated with a spectral acceleration that has a mean annual frequency of exceedance equal to P_0, an acceptable level for the limit state frequency (Figure 3-3). As it will be shown below, the demand factor in Equation 4-2 depends on a (second moment) statistical parameter of the demand and also on a parameter reflecting the sensitivity of demand to changes in the hazard level.

Once the probabilistic distribution parameters for demand (given spectral acceleration) are estimated, one can calculate the Factored Demand, defined as the product of median demand and the demand factor:

$$Factored\ Demand = median\ demand \times demand\ factor \qquad (4-3)$$

The formal equation for the factored demand will be discussed later in this chapter.

This chapter presents alternative methods for evaluating the factored demand. These methods will be introduced in the order of the amount of analysis effort they involve.

As it is mentioned above, the median demand term in Equation 4-3 in fact a conditional median for a given spectral acceleration level (Equation 3-13). Hence, the methods presented in this chapter are classified based on the range of the spectral acceleration values they cover, in their estimation of factored demand. The narrow-range methods estimate the factored demand over a narrow range of spectral acceleration values, e.g., around the spectral acceleration corresponding to the hazard level, P_0 (based on the formal equation for factored demand Equation 3-12). Single-stripe analysis and cloud analysis are two narrow-range methods that will be discussed in this chapter. Narrow-range methods involve a relatively small amount of analysis effort, at the price of providing only limited information about the factored demand. The wide-Range Methods tend to involve extensive analysis efforts and estimate the factored demand over a wider range of spectral acceleration values. These methods also permit limit state assessments over a wider range of spectral acceleration and limit state probability values. Multiple-stripe analysis and incremental dynamic analysis are the wide-range methods discussed in this chapter. This chapter will also use numerical integration to test the validity the analytical assumptions that form the basis of factored demand estimation.

4.4 A Comprehensive Assessment Example: An older reinforced concrete frame

We have selected an older reinforced concrete frame structure in Los Angeles, as a comprehensive case study in probabilistic assessment of an earthquake-damaged existing structure. This structure is serving as a test-bed for the activities of the PEER center. This chapter is also an effort in summarizing and classifying the results of our analyses on a model frame from this building.

For our probabilistic assessment purposes, the accuracy of the mathematical modeling of this particular building was not imperative. Nevertheless, we were interested in analysis software that would enable us to model the challenging issues of cyclic stiffness and strength degradation behavior in reinforced concrete. We employed DRAIN2D-UW that is a modified version of DRAIN2D that was produced by Professor Jose Pincheira's research team in the University of Wisconsin (see Pincheira et al., 1999 and Dotiwala et al., 1998).

We modeled one of the transverse frames using DRAIN2D-UW. Figure 4-1 illustrates the mathematical model of the frame:

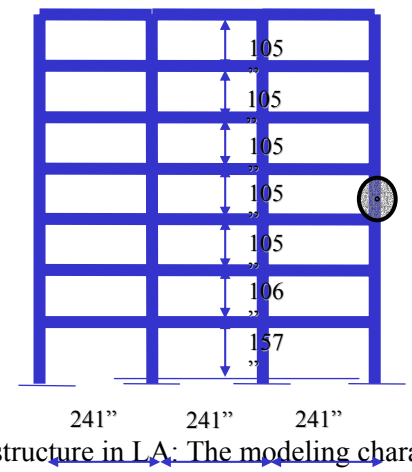

Figure 4-1 – A 7-story frame structure in LA: The modeling characteristics of a transverse frame

The members are modeled using a beam-column element. The degrading behavior is concentrated in two rotational springs at the two ends (flexure) and a translation spring somewhere in the middle of the element (shear). The hysteretic response of a beam-column element modeled by DRAIN2D-UW is shown in Figure 4-2. The degrading behavior observed in the plot reflects the degradation in both shear and flexure.

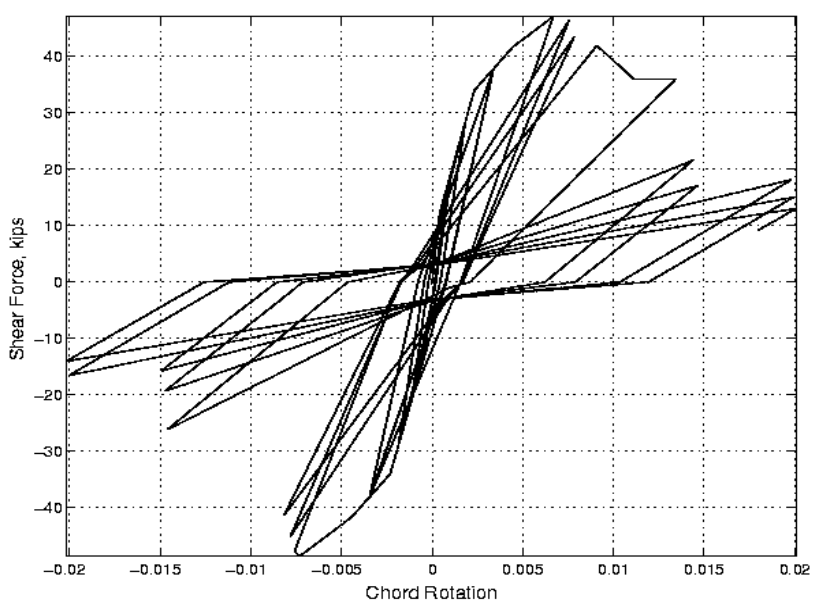

Figure 4-2 - Hysteretic response of a beam-column to cyclic loading.

The beam-column is modeled using DRAIN2D-UW

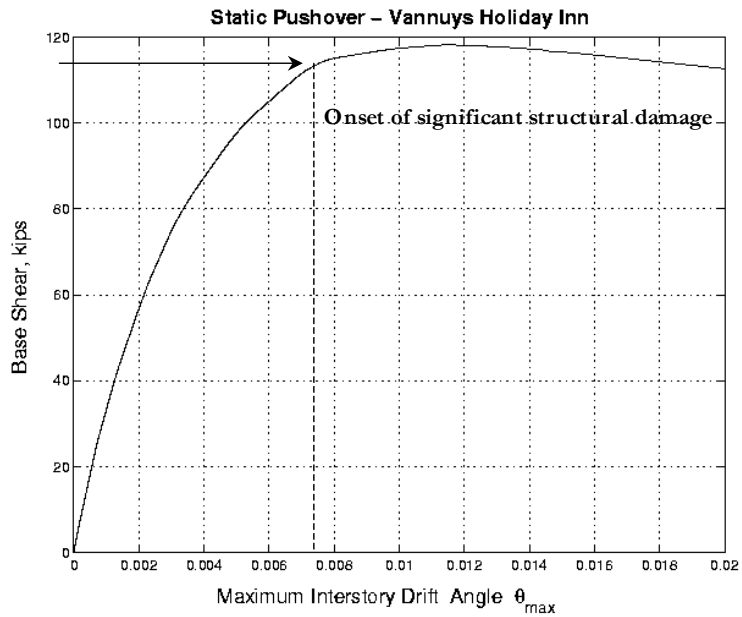

Figure 4-3 - The Static Pushover Curve for the Structural Model.

The static pushover curve for the structure is plotted in Figure 4-3. Note that it is plotted with respect, not to the customary roof rift, but to the response measure used here, maximum (over all stories) of the inter-story drift angle. The onset of significant structural damage (inter-story drift of 0.0075) in the frame is marked on the curve. It should be noted that the hysteretic model does not take into account a mode of axial of failure prompted by large shear forces in the columns, which is realistically expected to happen at drift values between 1-2% (see Moehle et al., 1994, Elwood and Moehle, 2002). Therefore, the analysis results in this chapter should be considered as, "conditioned on no other failure modes". Meanwhile, consideration of other potential modes of failure would be a challenging test of the accuracy of the methods presented in this chapter.

4.5 Record Selection

For this exercise a set of 30 ground motion records were selected from the Silva Catalog (Silva, 1998) for California Sites. These records were all California events recorded on stiff soil (Geo-Matrix soils types C and D) and were selected from a moment magnitude- (closest) source-to-site distance range of:

$$5.5 < M < 7.5$$
$$15 < R < 120 \quad km$$

Addressing the current issues in ground motion selection is not the focus of this study. It is generally presumed that one should select records representative of the events that dominate the probabilistic hazard for the ground motion levels of interest, as determined informally or formally, e.g., by disaggregation (see McGuire, 1995 and Bazzurro and Cornell,1998). This magnitude range, $5.5 \le M \le 7.5$, is presumed to be representative of the events likely to cause severe ground motions at this site. With the exception of potential near-source and directivity-influenced records, the most important record characteristics (e.g., spectral shape), other than general amplitude level, are comparatively insensitive to distance. In most cases in this study the records will be scaled relative to their recorded values; therefore the recorded amplitude is not directly relevant. Directivity issues (e.g., pulse-like records) are beyond the scope of this particular study (see, e.g. Alavi and Krawinkler, 2000; Luco and Cornell, 2001). Issues of nonlinear response sensitivity to magnitude and distance and record scaling are discussed by Shome et al. (e.g., Shome, et al., 1998; Shome and Cornell, 1999). Nonetheless the subject of site-specific record selection and modification for nonlinear demand estimation deserves, and is the subject of, further research.

4.6 Probabilistic Framework for Design and Assessment of Structures

Presented below is the continuous version of Equation 4-1 (and also Equation 2-2), with maximum inter-story drift angle denoted by $\theta_{\max}$, as the displacement-based demand. This equation is based on the assumption that capacity C_{LS} is statistically independent of S_a and $\theta_{\max}$ (see Section 2.5.7.4):

$$\lambda_{LS} = \int_y \int_x F_{C_{LS}}(y) \cdot f_{\theta_{\max}|S_a}(y \mid x) \cdot \left| \frac{d\lambda_{S_a}(x)}{dx} \right| \cdot dx \qquad (4\text{-}4\text{-a})$$

Where:

λ_{LS}	Mean annual frequency of exceeding a limit state, *LS*
C_{LS}	Capacity for the limit state, *LS* in displacement terms
$\theta_{\max}$	Demand in displacement terms
S_a	Intensity measure; here it is the first mode spectral acceleration
$F_{C_{LS}}$	Cumulative probability density function of capacity

$f_{\theta_{\max}\|S_a}$	Probability distribution function of the demand for a given level of S_a
λ_{S_a}	Spectral acceleration hazard, in terms of the mean annual frequency of exceedance
x	A given value of S_a
y	A given value of $\theta_{\max}$

While Equation 4-1 is very general with respect to the choice of ground motion intensity measure and demand variable, here, we have chosen to use the maximum inter-story drift angle within the structure, $\theta_{\max}$, as the demand variable in the design/assessment process. This is a particularly suitable choice for moment resisting frame structures, since it relates the global response of the structure quite directly to joint rotations where most of the inelastic behavior in the moment resisting frames is concentrated. We have used the spectral acceleration with the period of the fundamental mode of the structure, S_a, as the intensity measure variable. Studies by Shome and Cornell (e.g., Shome, et al., 1998; Shome and Cornell, 1999) show that for moment-resisting frame structures with their first-mode period lying within the moderate range (e.g., around T=1.0 sec), the spectral acceleration of first mode is sufficient for relaying the primary ground motion characteristics to the structural response.

4.7 Drift Hazard - the Annual Frequency of Exceeding Drift Demand

Equation 4-4-a can be re-written in the following manner:

$$\lambda_{LS} = \int_y \int_x F_{C_{LS}}(y) \cdot f_{\theta_{\max}|S_a}(y \mid x) \cdot \left| \frac{d\lambda_{S_a}(x)}{dx} \right| \cdot dx = \int_y F_{C_{LS}}(y) \cdot \left| \frac{d\lambda_{\theta_{\max}}(y)}{dy} \right| \cdot dy \qquad (4\text{-}4\text{-b})$$

where $\lambda_{\theta_{\max}}(y)$ is the (mean) annual frequency that drift demand, $\theta_{\max}$, exceeds the value, y. $\lambda_{\theta_{\max}}(y)$ can be calculated, using the same technique as the one used for the limit state frequency, from the expression below:

$$\lambda_{\theta_{\max}}(y) = \int_x G_{\theta_{\max}|S_a}(y \mid x) \cdot \left| \frac{d\lambda_{S_a}(x)}{dx} \right| \cdot dx \qquad (4\text{-}5\text{-a})$$

Where $G_{\theta_{\max}|S_a}(y\,|\,x)$ is the conditional complementary cumulative density function (CCDF) of demand, $\theta_{\max}$, for a given S_a value. We can derive the expression for $\left|d\lambda_{\theta_{\max}}(y)/dy\right|$ in Equation 4-4-b by taking the derivatives of both sides of Equation 4-5-a with respect to *y*:

$$\left|\frac{d\lambda_{\theta_{\max}}(y)}{dy}\right| = \int_x f_{\theta_{\max}|S_a}(y\,|\,x)\cdot\left|\frac{d\lambda_{S_a}(x)}{dx}\right|\cdot dx \qquad (4\text{-}5\text{-}b)$$

Where $f_{\theta_{\max}|S_a}(y\,|\,x)$ is the conditional probability density function (PDF) of demand, $\theta_{\max}$, for a given S_a value. The above derivation is based on the relationship between the PDF and the CCDF of a probability distribution (Equation 2-12). There is a complete discussion of drift hazard and its derivation in Chapter 2.

4.8 Demand and Capacity Factored Design Format

In order to derive a (codifiable) limit state safety checking format, we set the mean annual frequency of exceeding the limit state, λ_{LS}, in Equation 4-4 to less than or equal to a selected tolerable level, P_0. The following expression in Equation 4-6 is an explicit presentation of Equation 4-2, obtained upon making a series assumptions as discussed below. The derivation of Equation 4-6 is explained in detail in Chapter 3.

$$\eta_{C_{LS}}\cdot e^{-\frac{1}{2}\frac{k}{b}\cdot\beta^2_{C_{LS}}} \geq \eta_{\theta_{\max}|^{P_0}S_a}\cdot e^{\frac{1}{2}\frac{k}{b}\cdot\beta^2{}_{\theta_{\max}|S_a}} \qquad (4\text{-}6)$$

Where:

$\eta_{\theta_{\max}\|S_a}$	Median demand $\theta_{\max}$ for a given spectral acceleration, S_a (here in terms of the maximum inter-story drift angle)
$\eta_{C_{LS}}$	Median capacity (here in terms of the maximum inter-story drift angle)
$\beta_{\theta_{\max}\|S_a}$	Dispersion measure for demand given the spectral acceleration level, S_a
$\beta_{C_{LS}}$	Dispersion measure for capacity
P_0	Tolerable frequency of exceedance of the limit state
${}^{P_0}S_a$	The spectral acceleration associated with the annual frequency of exceedance equal to P_0

$\eta_{\theta_{\max}|^{P_0}S_a}$ Median value of $\theta_{\max}$ given a spectral acceleration equal to $^{P_0}S_a$

k The (log) slope of the hazard curve if it is approximated by a power-law function

b The (log) slope of the median displacement-demand versus spectral acceleration curve it is approximated by a power-law function

k/b A sensitivity factor reflecting the change in the probability with respect to the change in the displacement-based demand

$\eta_{\theta_{\max}|^{P_0}S_a} \cdot e^{\frac{1}{2}\cdot\frac{k}{b}\cdot\beta^2_{\theta_{\max}|S_a}}$:

Factored demand for an allowable (mean) annual frequency of exceeding the limit state capacity equal to P_0.

The exponential factors in Equation 4-6 represent the capacity and demand factors in Equation 4-2. A complete discussion of the assumptions made in the derivation of Equation 4-6 can be found in Chapter 2. Briefly, probability density functions for limit state capacity and the demand given spectral acceleration are assumed to be lognormal. The lognormal density function is defined by the median (the η term) and by the standard deviation of the natural logarithm (denoted β), called here the "dispersion measure" or the "fractional standard deviation". This measure is approximately equal numerically to the coefficient of variation (COV), i.e., for values of COV less than 0.2, one can assume that $COV^2 \approx \beta^2$ with less than 2% error in β^2 (Benjamin and Cornell, 1970). These parameters will be estimated from the data in the examples to follow.

Thus, the probability distribution for the capacity is defined by $LN(\eta_{C_{LS}}, \beta_{C_{LS}})$ and the probability distribution for demand given spectral acceleration is defined by $LN(\eta_{\theta_{\max}|S_a}, \beta_{\theta_{\max}|S_a})$. In order to carry out analytically the integrals presented above, and subsequently to derive Equation 4-6, it is presumed that spectral acceleration hazard curve and median demand-spectral acceleration relationship can be predicted, at least over a local region sufficiently wide to yield reasonable numerical accuracy, by power-law type expressions in the form of $\lambda_{S_a}(x) = k_0 \cdot x^{-k}$ and $\eta_{\theta_{\max}|S_a} = a \cdot S_a{}^b$, respectively. It should be noted that k and b are the slopes of $\ln \lambda_{S_a}$ versus $\ln S_a$ and $\ln \eta_{\theta_{\max}}$ versus $\ln S_a$ relationships.

We now focus our attention on the terms that constitute the expression for factored demand (based on Equations. 4-3 and 4-6):

$$Factored\ Demand = \eta_{\theta_{\max}|^{P_0}S_a} \cdot e^{\frac{1}{2}\cdot\frac{k}{b}\cdot\beta^2_{\theta_{\max}|S_a}} \qquad (4\text{-}7)$$

Verbally, the factored demand is equal to the product of the median demand, $\eta_{\theta_{\max}|^{P_0}S_a}$, for the motions within the given spectral acceleration level ${}^{P_0}S_a$ and the demand factor or the exponential term, $\exp(\frac{1}{2}\cdot\frac{k}{b}\cdot\beta^2_{\theta_{\max}|S_a})$, which is a function of the sensitivity factor, k/b, and the standard deviation of (the logarithm of) the demand for a given spectral acceleration (dispersion), $\beta_{\theta_{\max}|S_a}$. Hence, the evaluation of factored demand consists of finding ways to estimate $\eta_{\theta_{\max}|^{P_0}S_a}$, $\beta_{\theta_{\max}|S_a}$ and k/b. Since the dispersion measure and the sensitivity factor are both in the power of the exponential, they assume secondary roles as compared to the median.

Based on the same assumptions as discussed above, the drift hazard is derived as (the derivation of the following analytic form for the drift hazard can be found in Section 2.5.7.3):

$$\lambda_{\theta_{\max}}(x) = \lambda_{S_a}(S_a^x)\cdot e^{\frac{1}{2}\cdot\frac{k^2}{b^2}\cdot\beta^2_{\theta_{\max}|S_a}} = \lambda_{S_a}(\eta^{-1}_{\theta_{\max}|S_a}(x))\cdot e^{\frac{1}{2}\cdot\frac{k^2}{b^2}\cdot\beta^2_{\theta_{\max}|S_a}} \qquad (4\text{-}8)$$

Where S_a^x is denoted as the spectral acceleration that "corresponds" to a drift equal to *x*. More precisely, S_a^x is the inverse of $x = \eta_{\theta_{\max}|S_a^x} = a\cdot(S_a^x)^b$, i.e., $S_a^x = \eta^{-1}_{\theta_{\max}|S_a^x} = (x/a)^{1/b}$. This is the spectral acceleration value that has (approximately) a 50% chance of causing a drift response equal to or greater than *x*. $\lambda_{S_a}(S_a^x)$ is the spectral acceleration hazard value (the mean frequency of exceeding) for S_a^x. It is interesting that the drift hazard in Equation 4-8 can be calculated as the spectral acceleration hazard at a spectral acceleration value, S_a^x, times an exponential factor, $\exp(\frac{1}{2}\cdot\frac{k^2}{b^2}\cdot\beta^2_{\theta_{\max}|S_a})$, closely resembling the one for the factored demand, both are functions of the sensitivity factor, k/b, and the dispersion in demand for a given spectral acceleration, $\beta_{\theta_{\max}|S_a}$.

In order to calculate the drift hazard from Equation 4-8, we need to estimate $\eta_{\theta_{\max}|S_a}$, $\beta_{\theta_{\max}|S_a}$ and k/b and the spectral acceleration hazard curve λ_{S_a} for all spectral acceleration levels. Thus, the alternative methods discussed in this chapter achieve a two-fold objective of estimating the factored demand as well as the drift hazard curve.

Recalling from Section 3.2.3.5 in Chapter 3, factored demand happens to be the drift value that corresponds to the hazard level P_0 on the drift hazard curve. We will see later in this chapter that this particular relationship is going to be very useful for the calculation of factored demand in cases where there are no closed form solutions available for factored demand. One such example is when numerical integration is used to calculate the integrals in Equations 4-4 and 4-5 for drift hazard and the annual limit state frequency.

The methods discussed in this chapter estimate the three quantities above in alternative ways. Being a characteristic of the hazard rather than the structural response, the *k* value is estimated in a similar manner in all the methods. Hence, it suffices for each method to estimate $\eta_{\theta_{\max}|^{P_o}S_a}$, $\beta_{\theta_{\max}|S_a}$ and b.

4.9 Site Specific Hazard Curve: Estimation of k Value

The *k* value can be estimated from a site-specific or mapped regional basis spectral acceleration hazard curve, provided by earth scientists. A spectral acceleration hazard curve provides the mean annual frequency of exceeding a particular spectral acceleration for a given period and damping ratio. In order to estimate *k*, we fit a power-law type of expression to the hazard curve in the region of spectral acceleration values of interest as proposed by for example by development underlying Department of Energy Standard 1020 (see Kennedy and Short, 1994, and Luco and Cornell, 1998):

$$\lambda_{S_a}(s_a) \approx P[S_a \geq s_a] = k_0 \cdot s_a^{-k} \qquad (4\text{-}9)$$

Where k_0 and k are the fit parameters.

Figure 4-4 shows a firm soil site-specific hazard curve calculated for Van Nuys, CA, at T = 0.85 sec, T being the first natural period of the structure, plotted in a two-way logarithmic scale. The figure also shows the line fitted to the hazard curve in the region of interest, i.e., a power-law approximation in the arithmetic scale calculated around an annual frequency of about 1/1000. The (absolute value of) slope of the fitted line is the *k* value in the region of interest.

4.10 Evaluation of Factored Demand by Numerical Integration

So far, we have talked about approximate methods for demand estimation. Inevitably, the question arises as to how we can get a “true” estimate of the factored demand.

As mentioned before, the closed form solution for the factored demand is valid as long as the underlying assumptions hold. However, we can evaluate the integrals in Equations 4-4 and 4-5 by numerical integration even when those assumptions stop to be valid. Here, we have calculated the expression for drift hazard (Equation 4-5) by numerical integration and have plotted it versus the spectral acceleration in Figure 4-4.

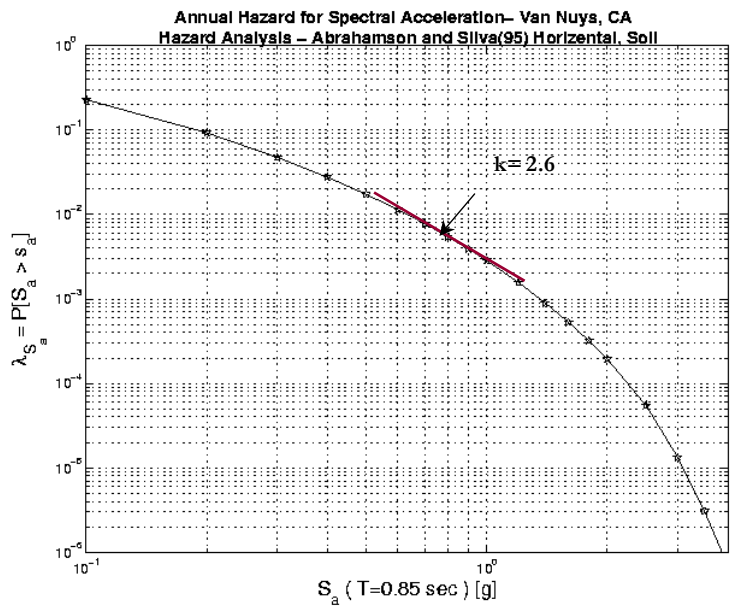

Figure 4-4 -Site Specific Hazard Curve, Van Nuys CA . Approximating the Hazard curve with a line in the region of interest.

We estimated the conditional complementary cumulative density function of demand for a given spectral acceleration, $G_{\theta_{\max}|S_a}(y\,|\,x)$ in Equation 4-5-a, by the ratio of the demand values that exceed the value, y, for a spectral acceleration equal to x (also known as Empirical Distribution, see Efron and Tibshirani, 1993). This is also an approximation in that the sample size is limited. The spectral acceleration hazard curve used is that in Figure 4-4, which is obtained by performing conventional probabilistic seismic hazard analysis (PHSA).

As we have mentioned previously, the factored demand for a tolerable probability level, P_0, can be calculated from the drift hazard curve. Therefore, we are going to find the factored demand using the drift hazard calculated by numerical integration.

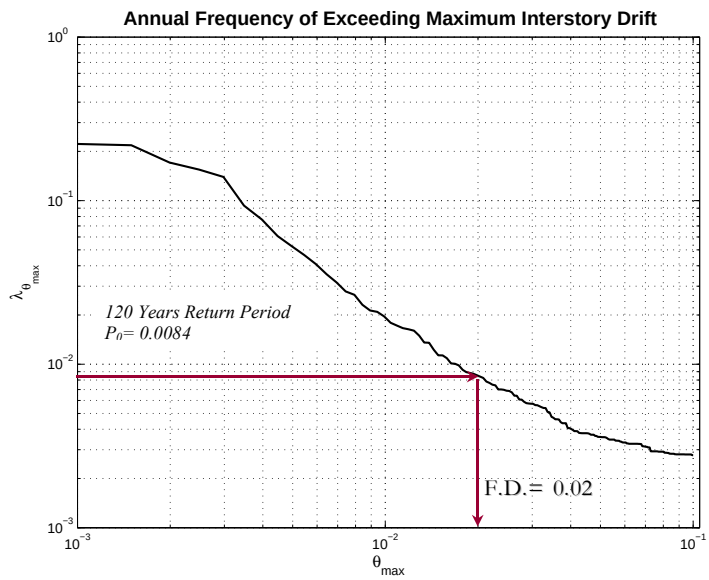

Figure 4-5 – The drift hazard curve derived by numerical integration. The factored demand corresponding to $P_0 = 0.0084$ is also shown on the plot.

As illustrated in Figure 4-5, we can use this curve to estimate the factored demand for a tolerable probability level, $P_0 = 0.0084$. This is a probability level that we believe is associated with the spectral acceleration levels that drive the structure to the verge of collapse (this particular probability level has been chosen merely for demonstration purposes). Therefore it is a severe test of the analytical approximation, permitting us to demonstrate its limitations under certain approaches. Later in the chapter, we are going to introduce another P_0 level that is associated with the onset of damage in structural members, $P_0 = 0.03$. At this level the analytical approximations will be found to be quite robust. In order to be consistent, we have used the same two values for P_0 throughout the chapter.

For a tolerable probability level of $P_0 = 0.0084$, the drift hazard curve yields a factored demand of, 0.02 (Figure 4-5), which corresponds to a ductility of 2 relative to the onset of significant structural damage.

In this chapter, we are going to refer to this quantity as the "true" factored demand for the tolerable probability $P_0 = 0.0084$. We are going to use this "true" factored demand as a measure for gauging each method's accuracy in factored demand estimation. Recall that the "true" value is

in itself an estimate because a sample size of "only" 30 records has been used to estimate $G_{\theta_{\max}|S_a}$ in Equation 4-5-a, and the hazard curve itself is an estimate.

4.11 Narrow Range Methods

Narrow range methods estimate the factored demand over a comparatively small neighborhood of spectral acceleration values. They require a relatively small number of analysis runs, at least compared to the methods that estimate the factored demand over wide ranges of S_a values.

However, these methods have a limited scope of application. They are especially effective in estimating probabilistic demand parameters that appear in the closed-form expression for the DCFD design format, e.g., Equation 4-6, over a targeted range of probability, ground motions, and displacements of interest.

4.11.1 Single-Stripe Analysis

The single-stripe analysis, as its name suggests, is a procedure that involves a structural dynamic analyses for a set of records scaled to a common spectral acceleration value.

The output of the single-stripe analysis, which is scattered along a stripe of constant spectral acceleration value, provides estimates for the median and dispersion of the inter-story drift demand conditioned on the spectral acceleration level of the stripe. The first question is what the appropriate spectral acceleration level for single-stripe analysis is. The answer depends on the criteria that are going to be satisfied.

The results of the single-stripe analysis are particularly well suited for estimating the factored demand, which is expressed as a function of ${}^{P_0}S_a$ or the spectral acceleration corresponding to the tolerable probability level P_0. This makes ${}^{P_0}S_a$ a potential candidate for the spectral acceleration level to which the ground motion records are scaled. Figure 4-6 illustrates how ${}^{P_0}S_a$ is calculated for an acceptable probability level of $P_0 = 0.0084$. The probability level, P_0, is marked on the hazard axis and its corresponding spectral acceleration value, ${}^{P_0}S_a$, is calculated by finding the S_a value that corresponds to a hazard level, P_0, via the hazard curve.

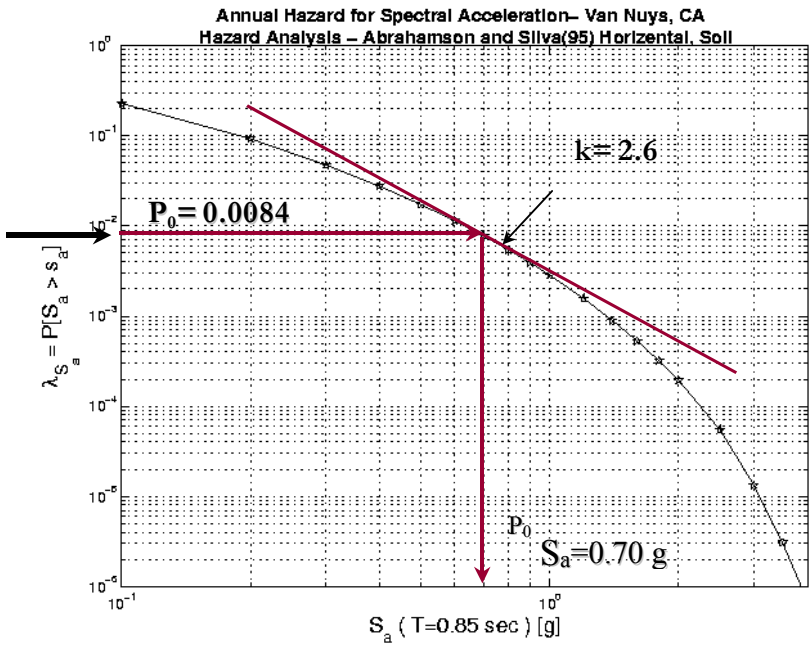

Figure 4-6 - The Spectral Acceleration Corresponding to an acceptable Probability Level of 0.0034

After choosing the spectral acceleration level of interest, in this case, ${}^{P_0}S_a = 0.70g$, the ground motion records are all scaled to this value. The scaled ground motions are then applied to the structure and the maximum inter-story drift demand values are calculated.

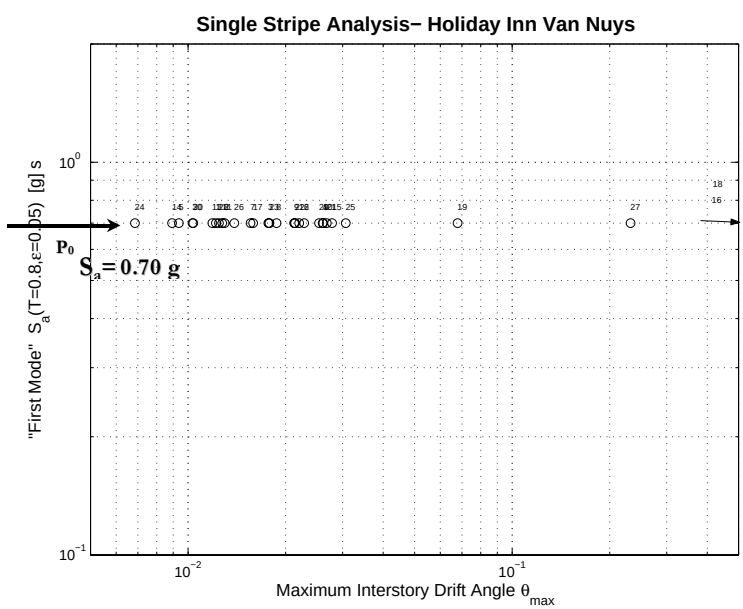

Figure 4-7 - "Stripe" response obtained by applying the selection of ground motion records scaled to the spectral acceleration of the stripe, ${}^{P_0}S_a = 0.70g$, to the model structure.

The "stripe" response of the model frame in Figure 4-1, subjected to the selection of ground motion records, is plotted against spectral acceleration in the logarithmic scale (Figure 4-7).

The statistical parameters of the "stripe" response can now be used to estimate the median and dispersion at the spectral acceleration level, ${}^{P_0}S_a$. Here we use the sample parameters denoted by $\hat{\eta}_{\theta_{\max}|S_a}$ and $\hat{\beta}_{\theta_{\max}|S_a}$ called, respectively, the "counted median" and the "counted standard deviation" of the "stripe" response for a given spectral acceleration level. In order to obtain the "counted" statistical parameters of a data set, the data is first sorted in the ascending order. The counted median is the 50th percentile of the sorted data. The counted standard deviation is estimated by the average of $\ln(\theta^{84th}/\theta^{50th})$ and $\ln(\theta^{50th}/\theta^{16th})$ respectively. The counted median and standard deviation for a spectral acceleration level, ${}^{P_0}S_a = 0.70g$, are calculated as 0.0183 and 0.49, respectively. These quantities are shown in Figure 4-8 (again in the logarithmic scale). We can observe that the displacement-based response is well into the strength degrading regime, explaining the comparatively large value $\hat{\beta}_{\theta_{\max}|S_a}$.

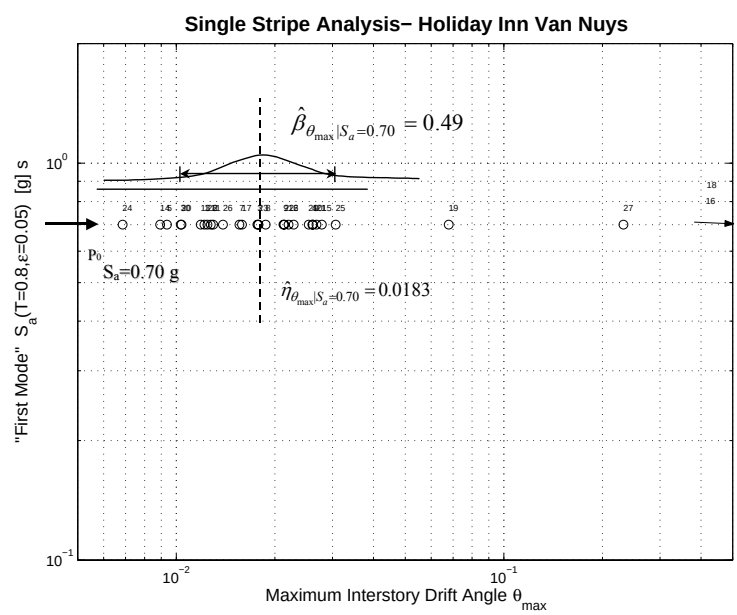

Figure 4-8 - Estimated Statistical Parameters for the *"Stripe"* Response

Once the statistical properties of the drift stripe response are calculated, they can be used as estimates of $\eta_{D|S_a}$ and $\beta_{D|S_a}$ (the method of moments can often be used as well, but difficulties will ensue if one encounters dynamic runs in which numerical convergence is not obtained,

and/or if very large, unrealistic displacements are computed.). The single stripe output does not provide displacement versus spectral acceleration slope information, i.e., the *b* parameter appearing in the expression for factored demand (Equation 4-7). As a preliminary estimate, we assume that the *b* value is equal to 1, implying that $\eta_{D|S_a}$ and S_a have a proportional relationship in arithmetic space. Elastic behavior and the "equal displacement rule" (see Veletsos and Newmark, 1960) are special cases of this condition. The factored demand estimate using the estimates of $\eta_{D|S_a}$ and $\beta_{D|S_a}$ obtained for single-stripe analysis method, is:

$$F.D. = \eta_{\theta_{\max}|^{P_0}S_a} \cdot e^{\frac{1}{2}\cdot\frac{k}{b}\cdot\beta^2_{\theta_{\max}|S_a}} = 0.0183 \times \mathrm{e}^{\frac{1}{2}\cdot\frac{2.6}{1}\cdot(0.49)^2} = 0.0183 \times 1.366 = 0.025$$

We can see that the single-stripe prediction for factored demand is equal to 0.025, which is much larger than the *"true"* factored demand, *F.D.=0.02*, in the previous section. In this case, because $\beta_{D|S_a}$ is relatively large, the demand factor is sensitive to the value of *b* and the single-stripe method with a default value of $b = 1$ produces a very conservative estimate of the factored demand. This brings up the question of how much extra analysis effort is required in order to enhance the results of single-stripe analysis method.

Next, we consider the efficiency of a double-stripe method, because the minimum number of stripes necessary for getting information about b value is two. As its name suggests the double-stripe method consists of two separate single-stripe analyses, the original single stripe analysis plus an additional stripe somewhat close to the original stripe at $^{P_0}S_a = 0.70g$. In this example we place the second stripe at $^{P_0}S_a = 0.80g$. The b value is estimated as the slope of the line on a log-log plot, that connects the medians of the two stripes:

$$b = \frac{\ln\left(\frac{\eta_{\theta_{\max|S_a=0.8}}}{\eta_{\theta_{\max|S_a=0.8}}}\right)}{\ln\left(\frac{0.8}{0.7}\right)} = 3.6$$

It should be noted that the estimates for $\eta_{D|S_a}$ and $\beta_{D|S_a}$ are the same as those obtained for the single stripe analysis above, i.e., the second stripe plays an auxiliary role for the purpose of estimating the b value. The results of a double-stripe method are plotted in Figure 4-9. The factored demand in this case is equal to:

$$F.D. = 0.0183 \times e^{\frac{1}{2} \cdot \frac{2.6}{3.6} \cdot (0.49)^2} = 0.0183 \times 1.09 = 0.020$$

The answer is very close to the "true" factored demand estimated by numerical integration. We should however note that the position of the second stripe, with respect to the original one- plays a critical role in estimation of the b value. If the second stripe is too far, the estimated *b* value may not be representative of the local slope around the original stripe. If it is too close, the estimated *b* value may fail to represent the general trend in spectral acceleration versus demand curve. Thus, the accuracy of a double-stripe analysis is dependant on the analyst's judgment in choosing the spacing between the stripes. A suggestion is to choose the second S_a stripe to be above the original value by a fraction (of that value) equal to $\frac{1}{4}$ or $\frac{1}{2}$ of $\beta_{D|S_a}$ (i.e., $S_a^2 = S_a^1 + fraction \cdot \beta_{D|S_a^1} \cdot S_a^1$).

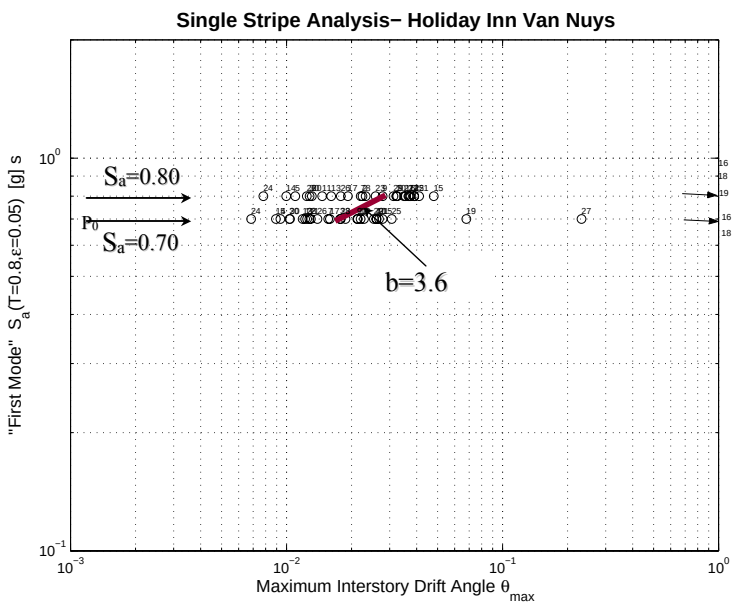

Figure 4-9 - Estimation of factored demand using two stripes, $\eta_{\theta_{\max}|S_a=0.80} = 0.03$

4.11.2 Cloud Analysis

The cloud analysis is a procedure in which a structure is subjected to a set of ground motion records of different first-period S_a values. In contrast to the single-stripe method, this method provides a "cloud" rather than a stripe of response values as shown in Figure 4-10.

This "cloud" response method provides estimates of the two statistical parameters of demand given the spectral acceleration, $\eta_{\theta_{\max}|S_a}$ and $\beta_{\theta_{\max}|S_a}$, as well as the b value. In its simplest form, the "cloud" response is obtained by applying original ground motions (as recorded) to the structure. If the ground motion records are taken from a bin (like the record selection in this chapter), they can represent an earthquake scenario defined by (M_{bin}, R_{bin}), the magnitude and distance representative of the bin.

Once the ground motion records are selected, they are applied to the structure and the resulting maximum inter-story drift angles are calculated. This provides a set of drift values that are the basis for cloud-method calculations. The response of the model frame when subjected to the set of (as recorded) ground motions is plotted in Figure 4-10.

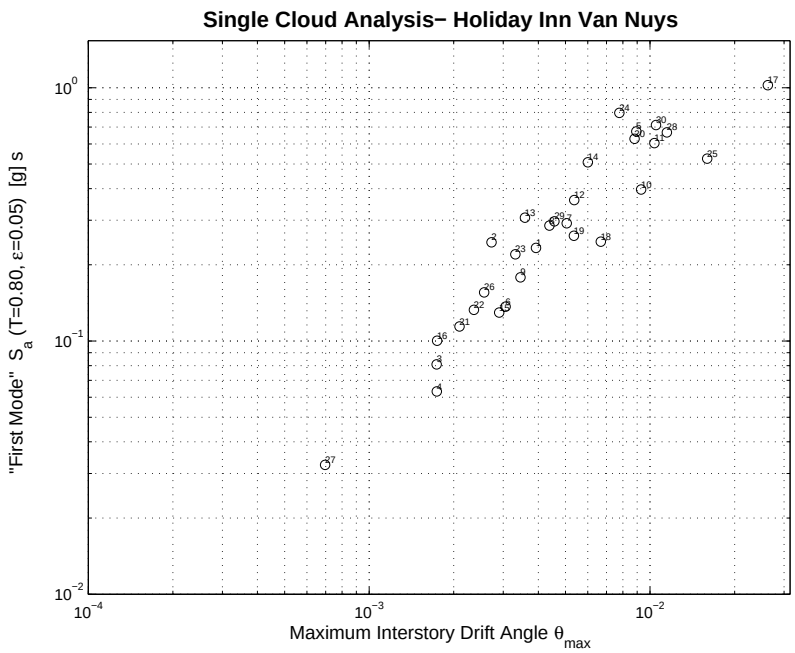

Figure 4-10– The "Cloud" Response of the Structure Subjected to a set of Ground Motion Records (plotted in the Logarithmic Scale).

In order to estimate the statistical properties of the "cloud" response, conventional linear regression (using least squares) is applied to the "cloud" response in the natural logarithmic scale, the standard basis for the underlying lognormal distribution model. This is equivalent to fitting a power-law curve of the form, $a \cdot S_a^{\,b}$, to the "cloud"

response in the original (arithmetic) scale. This results in a curve that predicts the median drift demand for a given level of structural acceleration:

$$\hat{\eta}_{D|S_a}(s_a) = \hat{a} \cdot s_a^{\hat{b}} \qquad (4\text{-}10a) \quad \text{or}$$

$$\ln(\hat{\eta}_{D|S_a}(s_a)) = \ln(\hat{a}) + \hat{b} \cdot \ln(s_a) \qquad (4\text{-}10b)$$

where $\ln(\hat{a})$ and $\hat{b}$ are linear regression constants. Detailed information about the estimation of the linear regression constants can be found in any applied statistics reference, such as, Benjamin and Cornell, 1970, or Rice, 1995. The results of such prediction can be used to estimate the median demand for a given spectral acceleration, $\eta_{D|S_a}$, for a specified spectral acceleration equal to ${}^{P_0}S_a$. The standard deviation of regression measuring the second moment of data points around the predicted curve can be used to estimate the dispersion measure, $\beta_{D|S_a}$:

$$\hat{\beta}_{D|S_a} = \sqrt{\frac{\sum(\ln(d_i) - \ln(\hat{a} \cdot s_{a,i}^{\hat{b}}))^2}{n-2}} \qquad (4\text{-}11)$$

Where d_i and $s_{a,i}$ are the drift demand and the corresponding spectral acceleration for record number *i* within the "cloud" response set and *n* is the number of records.

The standard deviation of regression, $\hat{\beta}_{D|S_a}$, as introduced in Equation (4-11), is presumed constant with respect to spectral acceleration over the range of spectral accelerations in the cloud. We will see later in this chapter that the dispersion measure, $\beta_{D|S_a}$, tends to increase for the larger values of spectral acceleration. Thus, assuming $\beta_{D|S_a}$ is constant, may be un-conservative in certain cases. This stresses the importance of performing linear regressions locally, i.e., in a region of spectral acceleration values of interest.

Figure 4-11 shows the median, $\hat{\eta}_{D|S_a}$, the dispersion, $\hat{\beta}_{D|S_a}$, and the *b* value, estimated (by fitting the cloud response) by linear regression. We can estimate the *b* value by the slope of the fitted

line in the logarithmic scale. The estimated *b* value here is in fact somewhat less than one, a phenomena commonly observed in the mild ductility region for moderate-period structures.

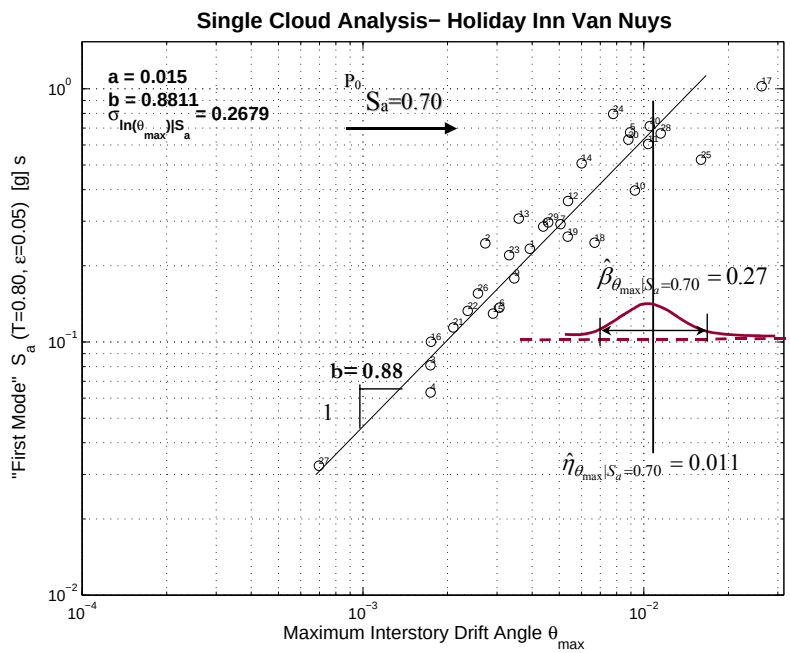

Figure 4-11 – The statistical properties of the "cloud" response. The parameter estimates for the median, $\eta_{D|S_a}$, and dispersion measure, $\hat{\beta}_{D|S_a}$, are shown on the figure.

The estimated $\hat{\eta}_{D|S_a}$, $\hat{\beta}_{D|S_a}$ and *b* values are finally used in to calculate the factored demand corresponding to $P_0 = 0.0084$ or ${}^{P_0}S_a = 0.70g$:

$$F.D. = \eta_{\theta_{\max}|{}^{P_0}S_a} \cdot e^{\frac{1}{2}\cdot\frac{k}{b}\cdot\beta^2_{\theta_{\max}|S_a}} = 0.011 \times e^{\frac{1}{2}\frac{2.6}{0.88}(0.28)^2} = 0.011 \times 1.12 = 0.012$$

Recalling from the previous sections, the "true" factored demand was calculated as 0.02, which is much larger than the prediction given by cloud analysis, 0.012. Thus, the cloud analysis is underestimating the drift demand in this case. This is can be due to the fact that the ground motion records used for the cloud analysis are not strong enough to properly represent the displacement-based response for spectral accelerations close to ${}^{P_0}S_a = 0.70g$.

4.11.3 Cloud Analysis Scaled

It is not easy to (a priori) find a selection of records that is representative of the displacement-based response in the vicinity of a given spectral acceleration level. for the cloud analysis method. Sometimes the records are not strong enough to represent the structural response in the region of displacement demands that we are interested in. In this example, we are interested in ground motions with a first-mode spectral acceleration around 0.70g, yet the set of ground motion records, as recorded, have a median S_a of only 0.27g. The median drift response, about 0.0045, corresponds to a ductility of only one with respect to the onset of significant structural damage. In order to get a more accurate estimate of the nonlinear response in the region of our interest, we have scaled the same collection of records by a factor of 2. We anticipate that the scaled cloud will more successfully capture the structural response in the range of S_a values around ${}^{P_0}S_a = 0.70g$.

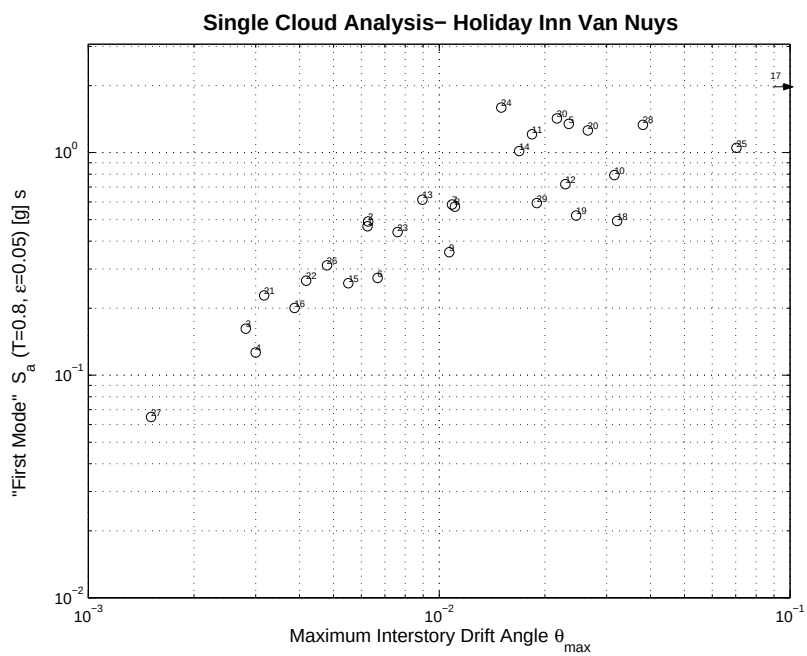

Figure 4-12– The scaled "cloud" response of the structure subjected to the selection of records, scaled by a factor of two.

As we can see in Figure 4-12, scaling has moved the cloud further up and to the right. Now that that the "cloud" response has become nearly centered around ${}^{P_0}S_a = 0.70g$, we expect the statistical information to be more representative of the demand level of interest we are estimating. The estimated statistical parameters for demand given spectral acceleration are plotted in Figure

4-13. As before, we have used linear regression to estimate the statistical properties of demand for a given spectral acceleration.

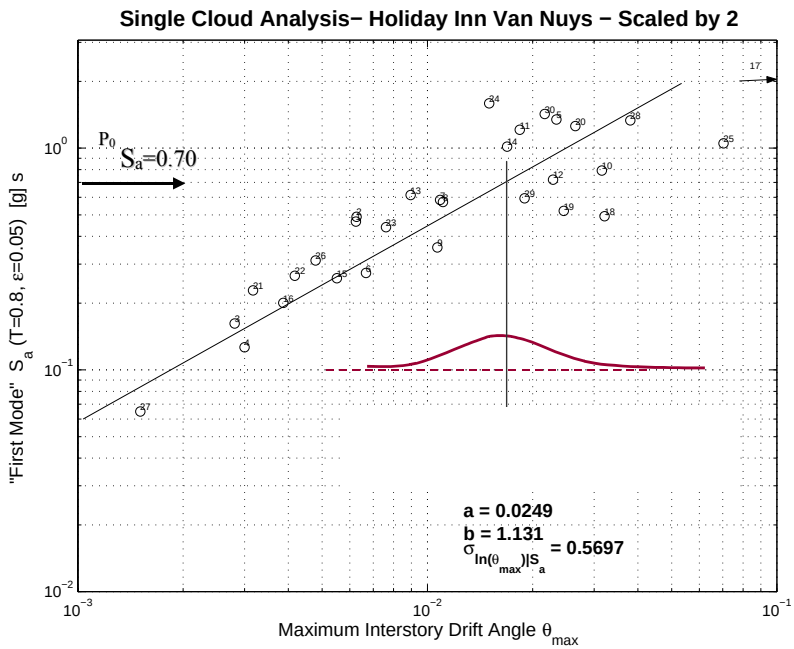

Figure 4-13 – The statistical properties of the "scaled cloud" response.

The estimated $\hat{\eta}_{D|S_a}$, $\hat{\beta}_{D|S_a}$ and *b values* – obtained from scaled cloud analysis - are incorporated below in the formula for factored demand:

$$F.D. = \eta_{\theta_{\max}|^{P_0}S_a} \cdot e^{\frac{1}{2}\cdot\frac{k}{b}\cdot\beta^2_{\theta_{\max}|S_a}} = 0.0166 \times e^{\frac{1}{2}\times\frac{2.6}{1.13}(0.57)^2} = 0.0166 \times 1.45 = 0.024$$

We see that in this case the scaled cloud method is still not capable of providing a highly accurate estimate for the factored demand for this S_a level. The factored demand estimate provided by this method is equal to 0.024, while the factored demand calculated by numerical integration is equal to 0.020. It is clear that it has produced adequate estimates of $\eta_{D|S_a}$, $\beta_{D|S_a}$ (compared to the locally more accurate results obtain from the stripe analysis) but its estimate of *b* remains too low; given the large value of $\beta_{D|S_a}$ the factor is in this case quite sensitive to *b*. As we shall see, b is changing in this range of S_a values and the regression can only provide a gross estimate. Nevertheless, this does meet to our preliminary expectation that, since the scaled ground motions

have spectral acceleration values closer to ${}^{P_0}S_a = 0.70g$, the scaled cloud would enhance the factored demand estimation.

4.11.4 Narrow-Range Methods for a Lower Spectral Acceleration ${}^{P_0}S_a = 0.40g$

We learned in the previous sections that, for ${}^{P_0}S_a = 0.70g$, the single-stripe analysis over predicted factored demand by 25%. We also learned that for the same S_a level of 0.70g, the single cloud analysis under predicted factored demand by 40%. Although the two methods are approximate, we know from closer inspection that their lack of accuracy here has been magnified by significant nonlinear behavior in S_a levels as high as ${}^{P_0}S_a = 0.70g$ and resulting irregularities in the response. In the next chapter we shall apply a scheme, introduced by Shome et al., 1998, in order to take into consideration the effect of having large displacements in the response.

In order to confirm this presumption, we have performed the two narrow-range methods, single-stripe analysis and single cloud analysis, for a lower spectral acceleration level. Thus, we have chosen a spectral acceleration equal to ${}^{P_0}S_a = 0.40g$, corresponding to a mean frequency level of $P_0 = 0.028$ or a return period of 33 years from the hazard curve in Figure 4-4. We can estimate the k value by the slope of the line fitted to the hazard curve in Figure 4-4, in the vicinity of $P_0 = 0.028$ This exercise yields a k value equal to 1.75.

Using the numerically integrated drift hazard curve in Figure 4-5, we can estimate the "true" factored demand, corresponding to a mean frequency level $P_0 = 0.028$. The so-called "true" factored demand is equal to 0.0080, which lies in the region of significant structural damage in the frame, with a ductility ratio around 1.0 (Figure 4-3). This roughly means that ${}^{P_0}S_a = 0.40g$ induces deformation and ductility levels that are approximately 40% of those of ${}^{P_0}S_a = 0.70g$ investigated as the primary example.

Single-Stripe Analysis on a Lower Stripe ${}^{P_0}S_a = 0.40g$ - The results of single-stripe analysis for a spectral acceleration level equal to ${}^{P_0}S_a = 0.40g$ are plotted in Figure 4-14. The statistical parameters for the "stripe" response are also illustrated on the figure. We have plotted this lower stripe on the same plot as the higher stripe of ${}^{P_0}S_a = 0.70g$ presented earlier. Assuming that the *b*

value is equal 1, and incorporating the estimated k value of 1.75, we have calculated the factored demand for ${}^{P_0}S_a = 0.40g$ below:

$$F.D. = \eta_{\theta_{\max}|{}^{P_0}S_a} \cdot e^{\frac{1}{2}\cdot\frac{k}{b}\cdot\beta^2_{\theta_{\max}|S_a}} = 0.007 \times \mathrm{e}^{\frac{1}{2}\cdot\frac{1.75}{1}\cdot(0.35)^2} = 0.007 \times 1.113 = 0.0078$$

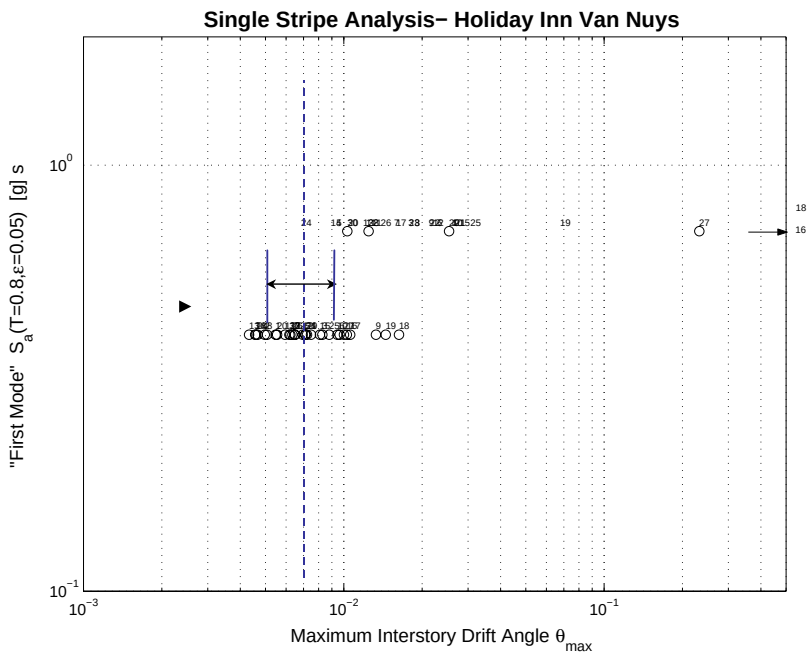

Figure 4-14 – "Stripe" response obtained by applying the selection of ground motion records scaled to the spectral acceleration of the stripe, ${}^{P_0}S_a$, to the model Structure.

This is very close to the "true" factored demand by numerical integration, 0.0080. This confirms our presumption that the narrow range methods provide more accurate estimates for lower spectral acceleration and deformation levels. Among other factors the lower levels of $\beta_{D|S_a}$ (e.g. 0.35 versus 0.49) make the exponential term closer to unity and less sensitive to b, k and $\beta_{D|S_a}$.

Cloud Analysis for ${}^{P_0}S_a = 0.40g$ - We can observe that the original "cloud" response in Figure 4-10 is roughly centered on spectral acceleration, ${}^{P_0}S_a = 0.40g$. Thus, we are going to use the original "cloud" response in Figure 4-10 in order to estimate the factored demand for a spectral acceleration of ${}^{P_0}S_a = 0.40g$. This provides the following estimates for $\eta_{D|S_a=0.40}$, $\beta_{D|S_a}$ and b:

$$\hat{\eta}_{D|S_a=0.40} = 0.0067$$
$$\hat{\beta}_{D|S_a} = 0.27 \qquad (4-12)$$
$$\hat{b} = 0.88$$

These are the same b and $\hat{\beta}_{D|S_a}$ values as for the ${}^{P_0}S_a = 0.70g$, since the b and $\hat{\beta}_{D|S_a}$ estimates provided by the single cloud analysis are constant for all spectral accelerations. We have calculated the factored demand below:

$$F.D. = \eta_{\theta_{\max}|{}^{P_0}S_a} \cdot e^{\frac{1}{2}\cdot\frac{k}{b}\cdot\beta^2_{\theta_{\max}|S_a}} = 0.0067 \times \mathrm{e}^{\frac{1}{2}\times\frac{1.75}{0.88}\cdot(0.27)^2} = 0.0067 \times 1.075 == 0.0072$$

This is within 10% of the *"true"* factored demand by numerical integration, $F.D. = 0.0080$.

4.12 Wide-Range Methods

Estimation of factored demand parameters over a wide range of spectral acceleration values requires relatively computation-intensive analysis efforts. This section presents a number of methods capable of estimating probabilistic demand parameters over such a range of spectral acceleration values. These methods have a larger scope of application compared to the narrow range methods. The wide range methods can map out the behavior of the system with respect to the range of possible future ground motions and a range of limit states probabilities. Thus, they can be used not just to check whether the failure probability is less than a specific tolerable level, P_o, but further, as will be shown, for the calculation of the limit state probability in cases where closed form solutions are not applicable.

Multiple-stripe analysis (MSA) is a collection of single-stripe analyses performed at multiple levels of the spectral acceleration. This will provide estimates of $\eta_{D|S_a}$, $\beta_{D|S_a}$ for each stripe as well as local estimates of the b value. This method is also helpful for calculating the frequencies of exceeding multiple structural limit states by numerical integration of Equation 4-4-a.

Incremental Dynamic Analysis is in essence the re-compilation of the results of multiple-stripe analysis into a collection of random entities known as the IDA curves. In other words, each ground motion record is successively scaled to multiple spectral acceleration levels and the resulting maximum inter-story drift angles are calculated in each case. The IDA curve connects the resulting inter-story drift angles corresponding to each ground motion record.

The IDA method also has the capability of extracting probabilistic information regarding the global instability collapse limit state. This feature will be employed for the evaluation of factored capacity of the collapse limit state, a step that completes the design/assessment process for this limit state.

4.12.1 Multiple-Stripe Analysis (MSA)

Scattered along multiple stripes of constant spectral acceleration, the results of multiple-stripe analysis can provide statistical information about the demand over a wide range of spectral acceleration values. Multiple "stripes" of response are obtained by applying to the structure a set of ground motion records that are scaled to multiple levels of spectral acceleration. The statistical properties of each stripe are obtained in the same way as the single-stripe analysis.

Figure 4-15-a illustrates the result of multiple-stripe analysis when the model structure is subjected to the same selection of the ground motion records mentioned before.

a) Plot in Arithmetic Scale *b) Plot in Logarithmic Scale*

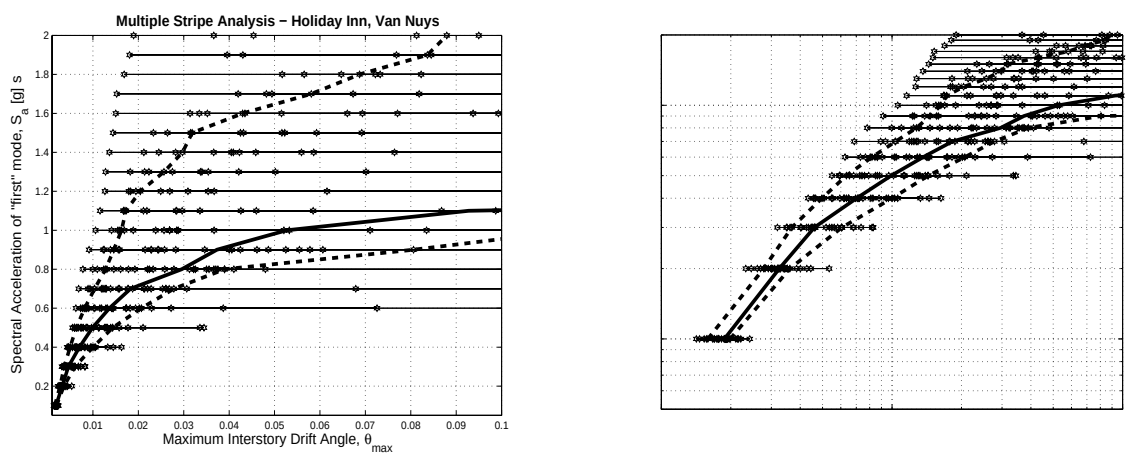

Figure 4-15 – Multiple-Stripe Analysis
(The same selection of records described in the beginning of the chapter)

The lines connecting the (counted) 16th, 50th and 84th percentiles of the stripes are also shown in Figure 4-15-a. Figure 4-15-b illustrates the same results in the logarithmic scale.

The median demand for a given spectral acceleration; $\eta_{D|S_a}$, can be estimated by the 50th percentile curve. Also, the dispersion measure, $\beta_{D|S_a}$, can be estimated (as a function of spectral acceleration) with the average band width created by 16th, 50th and 84th percentiles in the logarithmic plot. Finally, the *b* value can be estimated as the local/tangent slope of the (log-log) median curve for a given spectral acceleration value.

The multiple-stripe method provides a much more complete picture as to how both the general trend (median) and the dispersion of the response evolve under gradually increasing ground motion levels. Between about 0.80g and 1.1g, the median of the response "softens" rapidly and the dispersion increases markedly. The large dispersions beyond 1.0g imply that the median cannot be well determined even with 30 records.

Figure 4-16 illustrates the application of multiple-stripe analysis in the estimation of factored demand for a spectral acceleration equal to ${}^{P_0}S_a = 0.70g$. The factored demand at a spectral acceleration equal to ${}^{P_0}S_a = 0.70g$, can be calculated using the estimates for $\hat{\eta}_{D|S_a}$, $\hat{\beta}_{D|S_a}$ and *b* values as shown in Figure 4-16:

$$F.D. = \eta_{\theta_{\max}|{}^{P_0}S_a} \cdot e^{\frac{1}{2}\cdot\frac{k}{b}\cdot\beta^2_{\theta_{\max}|S_a}} = 0.0183 \times \mathrm{e}^{\frac{1}{2}\frac{2.6}{2.70}(0.49)^2} = 0.0183 \times 1.12 = 0.0205$$

Comparing the result with the "true" factored demand calculated before, $F.D. = 0.020$, it is clear that MSA method estimates the factored demand very closely. The only difference between using single stripe analysis and MSA here is local estimation of *b* value in the latter case. This emphasizes the importance of estimating the slope information, *b* value, in the region of interest, at least when $\beta_{D|S_a}$ is large, causing the factor to differ significantly from unity. It should be noted that the estimate for b value here is "more local" than from the one obtained from the double-stripe method.

It is possible to obtain accurate results more efficiently by performing MSA first with broader spacing and then filling in extra stripes where the *b* value is found to be changing comparatively rapidly. Also, as will be discussed further below, it would be advantageous to use more records when the dispersion is large and fewer records when dispersion is small.

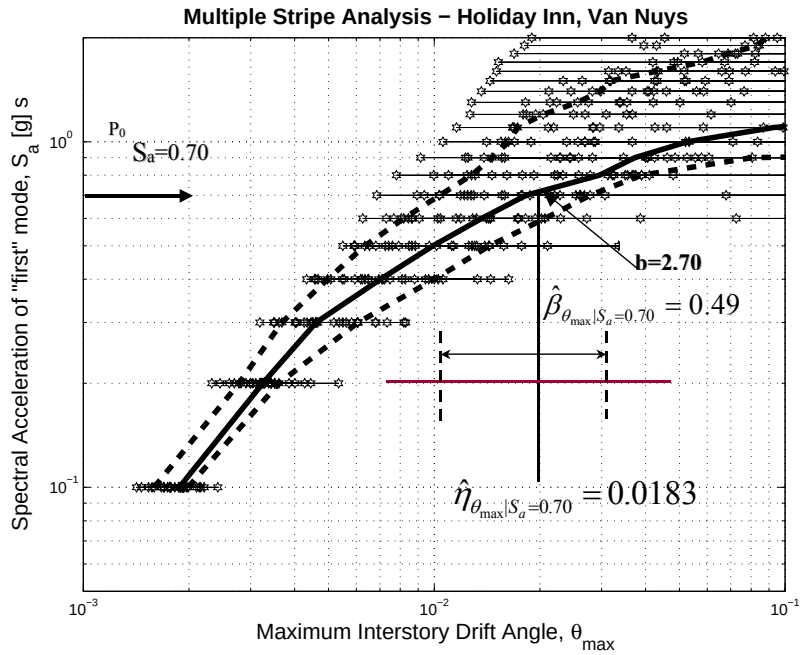

Figure 4-16 - Evaluation of factored demand by multiple-stripe analysis.

We have used the multiple-stripe analysis and the analytical approximations for factored demand to get the factored demand for different tolerable limit state frequencies.

The results of the multiple-stripe analysis and the analytical factored demand estimate for multiple levels of spectral acceleration are plotted in Figure 4-17 below versus the probability corresponding to these S_a levels, yielding an estimate of the drift hazard curve. The figure also illustrates the "true" factored demand as it is obtained by numerical integration. We can see that for drift values less than or equal 0.03, the MSA method prediction of factored demand is very close to the "true" factored demand calculated by numerical integration.

4.12.2 **Incremental Dynamic Analysis**

As described above, each IDA curve corresponds to a particular ground motion record and passes through maximum inter-story drift results obtained for the record scaled to multiple levels of spectral acceleration. Figure 4-18 illustrates individual IDA curves for two different records.

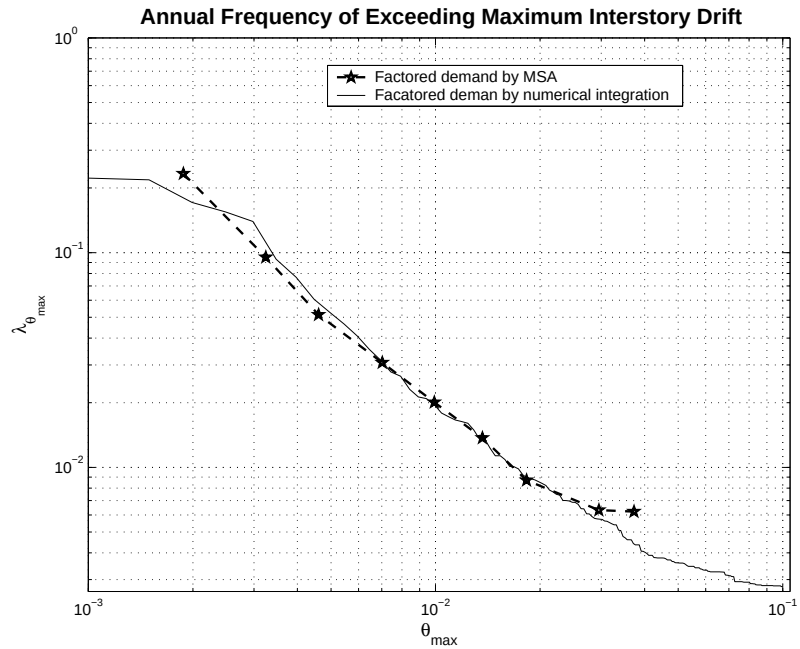

Figure 4-17 - Factored Demand predicted by Multiple-stripe Analysis (MSA) for Multiple Limit State Frequency Values, P_o, and the Drift Hazard Curve Obtained by Numerical Integration.

As it can be seen from Figure 4-18 below, the IDA curve gives a "richer" picture of how structure responds to different records, e.g., the "benign" nature of some records (Figure 4-18-b), and the "aggressive" nature of others (Figure 4-18-a).

a) IDA curve with "aggressive" behavior b) IDA curve with "benign" behavior

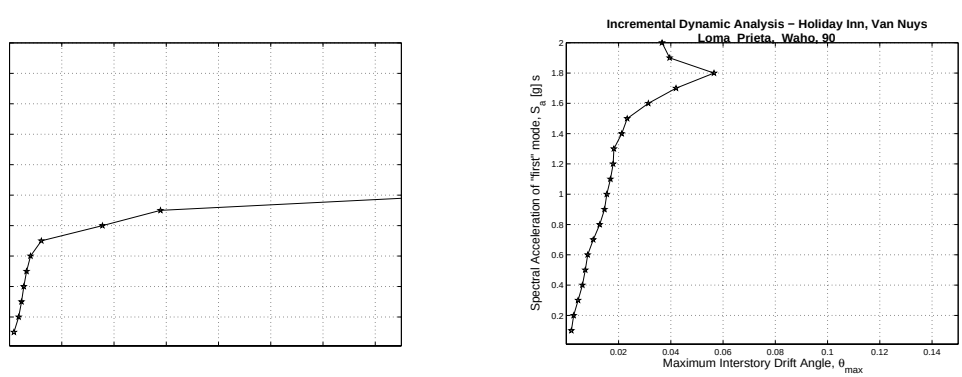

Figure 4-18- Individual IDA Curves

One can use curve fitting routines such as "the spline fit " in order to get smooth IDA curves (see Vamvatsikos and Cornell, 2002). With the IDA's, the percentiles of response can now be calculated as continuous curves, e.g., the median IDA curve or the 84th IDA curve (Figure 4-20).

In contrast to MSA method which is constructed by a collection of spectral acceleration stripes, the IDA curve can be constructed by scaling the records to arbitrary spectral acceleration values. This feature is useful when one is exploring different choices of Intensity Measures (IM) based on the same analysis runs. On the other hand, one can use different record sets for different levels in the MSA method, reflecting for example higher magnitudes at higher levels.

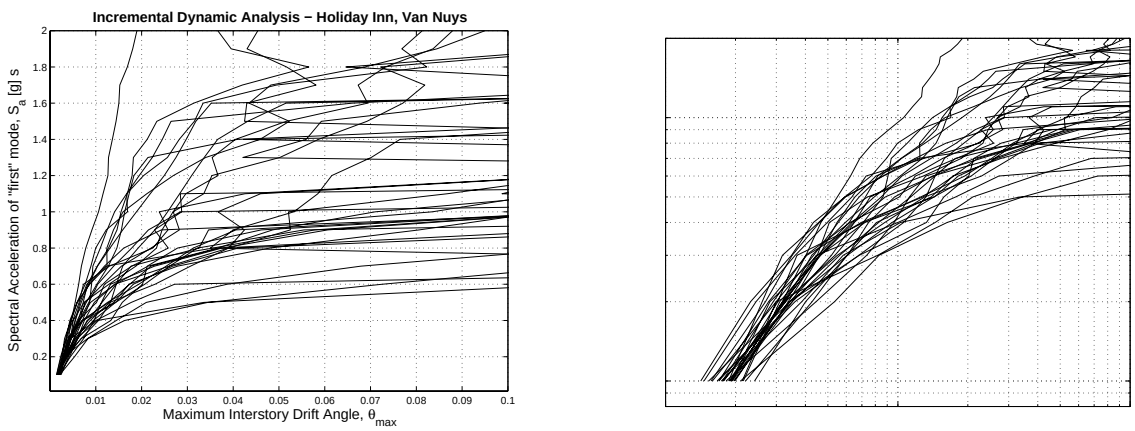

a) Plot in arithmetic scale b) Plot in logarithmic scale

Figure 4-19 – Results of the Incremental Dynamic Analysis when the model structure is subjected to the selection of ground motion records.

The application of IDA method in factored demand evaluation is illustrated in Figure 4-20. Factored demand can be calculated using the estimated values for $\eta_{D|S_a}$, $\beta_{D|S_a}$ and b value showed in Figure 4-20:

$$F.D. = \eta_{\theta_{\max}|^{P_0}S_a} \cdot e^{\frac{1}{2}\cdot\frac{k}{b}\cdot\beta^2_{\theta_{\max}|S_a}} = 0.0183 \times \mathrm{e}^{\frac{1}{2}\frac{2.6}{2.70}(0.49)^2} = 0.0183 \times 1.12 = 0.020$$

As expected, the results are identical to those of MSA method. Similar to MSA analysis, IDA method provides a good estimate of the factored demand.

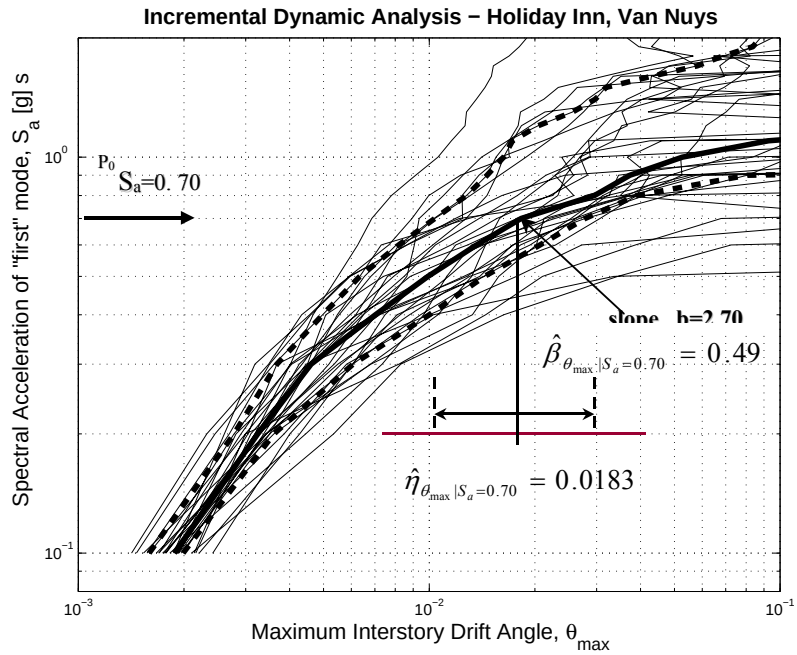

Figure 4-20 - Evaluation of the factored demand using the results of incremental dynamic analysis.

4.12.2.1 Capacity Estimation Using the Results of Incremental Dynamic Analysis-

The IDA method can also be used to obtain global instability (capacity) information about the structure. By global stability we mean a mode of collapse that is indicated by global dynamic instability in displacement response, i.e., the displacements increase an arbitrarily large amount for arbitrarily small increases in ground motion intensity. This particular mode of collapse can be captured from the results of an IDA. Following the definition in the FEMA/SAC Guidelines (see FEMA 2000), we have implemented this notion by marking the onset of this failure mode below (Figure 4-21) by a point where the local slope of the IDA curve decreases to a "certain percentage" of the initial slope of the IDA curve in the elastic region. This certain percentage is a more or less arbitrary value that represents the point where the IDA curve becomes "flat" enough; here, as in the FEMA/SAC Guidelines, we have chosen it to be equal to 20%. We can clearly observe the scatter in the capacity points for the different records in Figure 4-21.

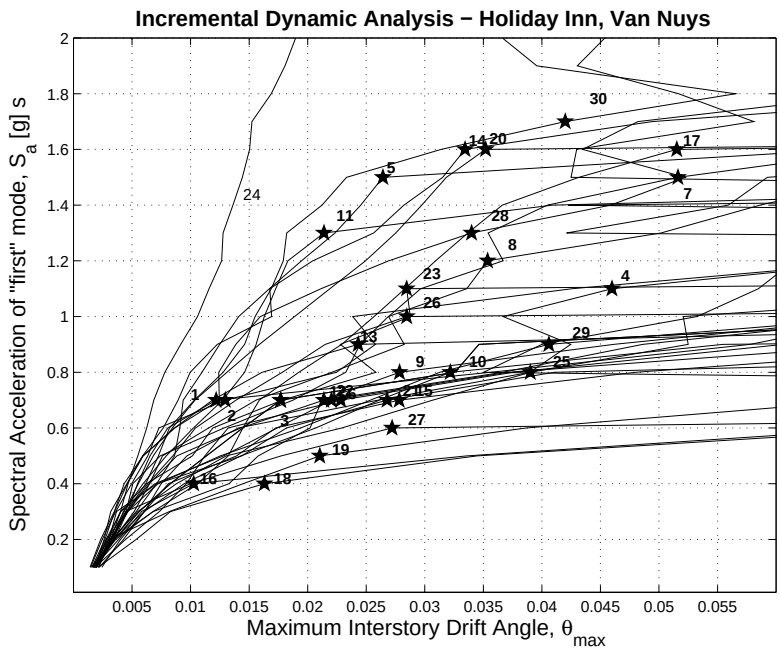

Figure 4-21 - "Collapse Points" marked on the IDA curves.

The statistical properties of the so-called collapse points are shown in Figure 4-22. Similar to factored demand estimation, this information can be used for estimating the factored capacity as:

$$F.C. = \eta_{C_{LS}} \cdot e^{-\frac{1}{2}\frac{k}{b}\cdot\beta^2_{C_{LS}}}$$

Note that we have used the b value here equal to 4, which is the local slope of the median curve in the vicinity of the drift capacity, $\hat{\eta}_{\theta_{cap}} = 0.0278$. Alternatively, the value associated with the level ${}^{P_0}S_a$ may be used.

$$F.C. = \eta_C \cdot e^{-\frac{1}{2}\frac{k}{b}\cdot\beta^2_C} = 0.0278 \times \mathrm{e}^{-\frac{1}{2}\frac{2.6}{4}(0.41)^2} = 0.0278 \times 0.95 = 0.026$$

Now that we have calculated the factored capacity, we can compare it with the factored demand that is estimated by multiple-stripe analysis or incremental dynamic analysis. Multiple-stripe analysis estimated the factored demand to be equal to, 0.020, which is smaller than the factored capacity, 0.026. This, according to DCFD design format (Equation 4-6), means that the annual frequency of collapse is less than the selected target value of 0.0084.

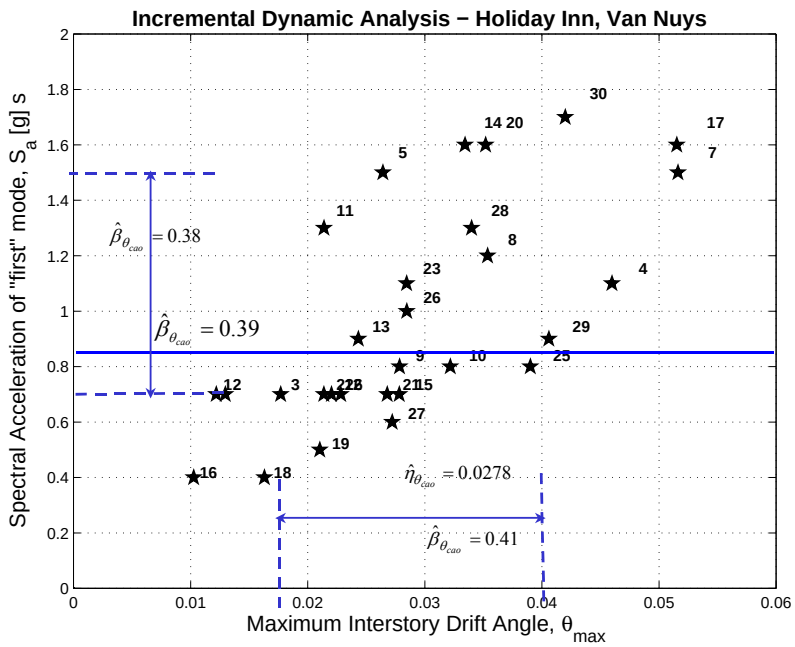

Figure 4-22 - Evaluation of the factored capacity using the results of incremental dynamic analysis (IDA)

4.12.3 Evaluation of Factored Capacity by Numerical Integration

For comparison we can also use numerical integration to estimate the factored capacity. First, we calculate the annual frequency of exceeding the global collapse limit state, λ_{LS}, by numerical integration (Equation 4-4-a). We have estimated the cumulative distribution function of collapse limit state, $F_{C_{LS}}(y)$, in Equation 4-4-a by the ratio of the capacity values that exceed the value, y, in the sample of capacity values obtained in the previous section (i.e., by the empirical distribution). The rest of the integration procedure is very similar to the calculation of drift hazard by numerical integration in the beginning of this chapter.

Now we need to transform the annual frequency of exceeding the collapse limit state into factored capacity format. According to the DCFD format, at the onset of collapse limit state, the factored capacity is equal to factored demand, i.e. the inequality in Equation 4-2 becomes equality. Therefore, the factored capacity is equal to the factored demand corresponding to a P_0 level equal to the limit state frequency, λ_{LS}. This means finding the drift value that corresponds to, λ_{LS}, from the drift hazard curve in Figure 4-5.

The annual frequency of exceeding the collapse limit state, λ_{LS}, which is calculated by numerical integration, is equal to 0.0063. This corresponds to a (factored) drift value equal to, 0.026, from the drift hazard curve in Figure 4-5. Thus, the "true" factored capacity is equal to factored demand for $P_0 = 0.0063$ from the drift hazard curve, 0.026. Similar to the factored demand calculated by numerical integration, the accuracy of the numerical integration can be increased by using larger number of records and by choosing broader integration limits. We can also recall that the factored capacity estimated by incremental dynamic analysis method was equal to 0.026.

4.13 Number of Records

In this chapter we have investigated alternative methods for demand estimation. All the methods were based on the original sample of 30 records. In this section, we discuss the effect of the sample size, e.g., the number of records for the single-stripe method. The effect of sample size for the other methods can be studied in the same manner.

We have conducted the single-stripe method with 30 ground motion records at ${}^{P_0}S_a = 0.70g$. This selection of 30 records can also be regarded as a sample of 30 earthquake scenarios, magnitude and distance pairs, that we have chosen out of the set of all possible earthquake scenarios for a given site. Here, we have conducted a bootstrap procedure (Efron and Tibshirani, 1993) on the sample in order to estimate the uncertainty in the estimation of median demand for a given spectral acceleration as a function of the sample size.

We generated numerous (n=500) replications, also known as boot strap replications, of sub-samples of size n (n is less than or equal to 30) by re-sampling with replacement. Each replication provides an estimate for the median drift for the given spectral acceleration level. The median and standard deviation of these median estimates were calculated for all the bootstrap replications for each sample size n. Figure 4-23-a illustrates the 500 observed median estimates from the bootstrap replications for each sub-sample size n (number of records). We can observe that the estimates of the median are more scattered (individually less reliable), as the number of records gets smaller. This reflects the typical sample size concern.

The standard deviation of the median of the bootstrap replications measures the uncertainty in the estimation of the median drift demand for a given spectral acceleration. Figure 4-23-a also illustrates the 16th, 50th and 84th percentiles of estimate of the median drift for a given spectral

acceleration (obtained by bootstrap analysis) as a function of the number of records used in order to estimate the median. The standard deviation of the median of the bootstrap replications can be presented by the width of the band created by the 16th and 50th and 50th and 84th percentiles (Figure 4-23-b).

As we mentioned above, the standard error in the estimation of the median is a measure of uncertainty in median due to limited sample size, i.e., number of ground motion records. We can observe that the standard error in the estimation of median drops with the increase in the sample size. This increase is (roughly) inversely proportional to square root of the number of records, as one would expect from simple statistical theory. Further, as a fraction of the median, the standard error of estimation is equal to $\frac{\beta_{D|S_a}}{\sqrt{n}}$ (Rice, 1995). The results shown are for ${}^{P_0}S_a = 0.70g$ when $\beta_{D|S_a}$ is 0.49. We see that in this case to reduce the standard error of the estimate of median to less than 20% will require a sample size of 12 or more.

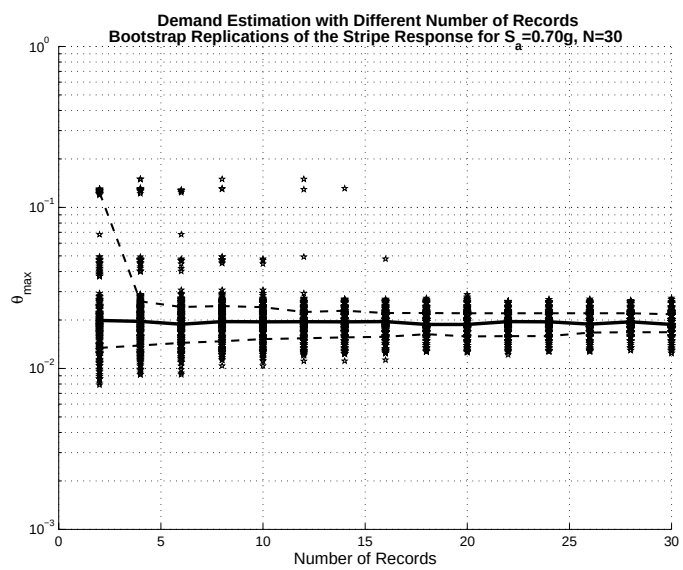

Figure 4-23-a) Median and standard error of the estimates of the median response as a function of the sample size (number of records). The straight line is the median response for each sample size. The 84th and 16th percentiles of the estimator of median response are also plotted in the figure.

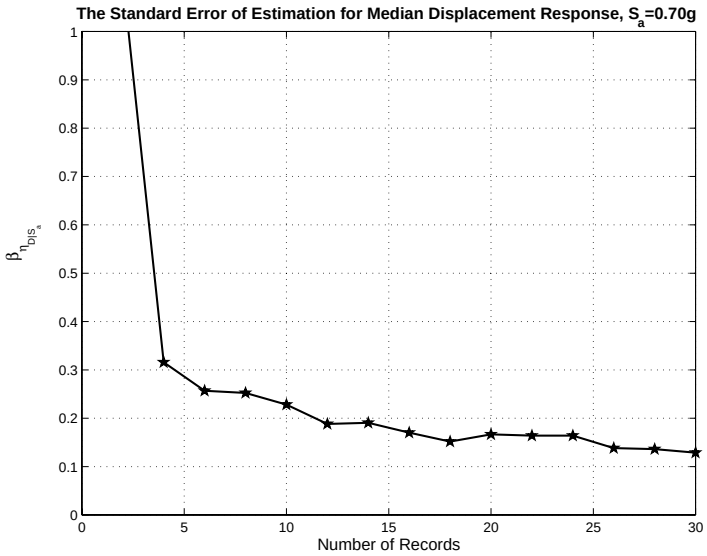

Figure 4-23-b) The (fractional) standard error of the estimates of median response as a function of the sample size (number of records).

4.14 Summary and Conclusions

Estimation of the engineering demand parameter (here, the displacement-based demand) is an essential part of the Demand and Capacity Factored Design (DCFD) procedure. This chapter presents alternative methods for the estimation of the factored demand, a displacement-based demand measure in the context of the DCFD format. These methods employ the results of non-linear dynamic analysis for displacement demand estimation. The methods are presented through a comprehensive case study of an existing reinforced concrete 7-story frame structure in Los Angeles. This structure represents an older reinforced concrete structure with degrading behavior in nonlinear range. The dynamic analyses are performed on a set of ground motion records selected from a catalog of California events recorded on stiff soil. The spectral acceleration of the first mode has been chosen as the representative ground motion intensity measure. The methods were divided into narrow-range and wide-range, with respect to the range of spectral acceleration values for which they provide estimations for the factored demand. The factored demand calculated by numerical integration, also referred to as the "true" factored demand, was used as a basis for comparison of the alternative methods, which are based on analytical integrations.

Single-stripe analysis and cloud analysis were the two narrow range methods presented in this chapter.

Single-stripe analysis method provided accurate estimations of the median displacement demand for a given spectral acceleration, $\eta_{\theta_{\max}|^{P_0}S_a}$, and the dispersion measure for the displacement for a given spectral acceleration, $\beta_{\theta_{\max}|^{P_0}S_a}$. However, it was unable to provide an estimate of the b value. While this estimate was satisfactory at lower ductility levels it led to a significant error at near collapse ductility levels. The factored demand was estimated assuming a default *b* value of 1. The estimated factored demand was much larger than the factored demand calculated by numerical integration because both $\beta_{\theta_{\max}|^{P_0}S_a}$ and *b* are large in such cases.

In order to enhance the factored demand estimation by single-stripe analysis, the double-stripe analysis method was introduced. This method consisted of performing another single-stripe analysis "sufficiently close" to the original stripe in order to provide a reasonable estimate of the log-log slope b value. For the near capacity ground motion level ($^{P_0}S_a = 0.70g$), the factored demand that was calculated using the estimated b value became much closer to the factored demand calculated by numerical integration. The improvement in the estimation of factored demand can be totally attributed to a fairly accurate estimation of the b value in the double-stripe method. At the higher levels of $\beta_{\theta_{\max}|S_a}$ associated with high ductility levels, the factored demand is much more sensitive to any error in *b*. This stresses the importance of estimating the b value in the region of interest. As seen in Figure 4-14-b the log-log slope changes at higher ground motions.

Cloud analysis using the ground motions "as recorded", while accurate at the lower deformation level, provided an estimate for the factored demand that was much smaller then the factored demand calculated by numerical integration for the higher S_a level. It failed to estimate the median demand well and underestimated $\beta_{\theta_{\max}|S_a}$.

In order to make the cloud response nearly centered on the spectral acceleration of 0.70g, the ground motion records were scaled by a factor of two. The cloud analysis using the scaled ground motions provided conservative estimate of the factored demand. Nevertheless, scaling the ground motions did enhance the factored demand estimation to some extent. The median, $\beta_{\theta_{\max}|S_a}$ and b values are all closer to the more extreme values at $S_a = 0.70g$. Cloud analysis by its very nature cannot provide good local estimates of those parameters when they are changing rapidly.

As wide-range methods, multiple-stripe analysis and incremental dynamic analysis were studied in the chapter.

Multiple-stripe analysis provided an accurate estimate of the factored demand for the extreme spectral acceleration of 0.70g. Comparing the multiple-stripe analysis and single-stripe analysis procedures for estimating the factored demand, it can be observed that everything is similar except for the estimation of the b value. Like the double-stripe analysis, the multiple-stripe analysis estimated the b value equal to the slope of the line connecting the median values for two adjacent stripes close to the spectral acceleration of 0.70g. Whereas, the single-stripe method could not provide an estimate of the *b* value. An accurate estimation of the b value may be essential for getting an accurate estimation of factored demand, especially if $\beta_{\theta_{\max}|S_a}$ is large.

Multiple-stripe analysis was applied to estimate the factored demand for multiple limit state levels, i.e., multiple spectral acceleration levels. Generally, multiple stripe analysis provided accurate estimates of the factored demand. The resulting factored demand estimations drifted away from the "true" factored demand when the (estimated) median demand became (unrealistically) non-smooth. In the next chapter, we will address these issues more carefully.

Incremental dynamic analysis provided results virtually identical to that of the multiple-stripe analysis. Compared to multiple-stripe analysis, the incremental dynamic analysis carries additional information about individual ground motion records by means of the IDA curves. The IDA curves follow the structural response to individual records as the spectral acceleration increases. These curves can be used to mark the onset of global instability for each ground motion record.

The onset of global dynamic instability (collapse) for each record, i.e., the collapse point, was marked on the corresponding IDA curve. The criteria for determining this threshold may change (see Vamvatsikos and Cornell, 2002).

The factored capacity, a displacement capacity measure in the context of the DCFD format, was estimated using the collapse points extracted from the IDA curves. The estimated factored capacity was found to be equal to the factored capacity as calculated from the numerical

integration. The estimated factored demand for a spectral acceleration of 0.70g was smaller than the estimated factored capacity for global dynamic instability (collapse) limit state. Therefore, according to DCFD format, annual failure probability is confirmed to be less than 0.0047.

In the final section of this chapter, the issue of uncertainty in the estimation of median drift due to limited sample size, i.e., n=number of records, was briefly discussed. The Bootstrap procedure, based on the original selection of records, was used to estimate the standard error in the estimation of the median drift that was provided by the single-stripe analysis.

It was confirmed that in fractional terms the standard error in the estimation of median drift provided by single-stripe analysis is approximately equal to $\beta_{\theta_{\max}|S_a} / \sqrt{n}$. Therefore the required sample size to achieve a pre-set "accuracy" in the median demand (and roughly, the factored demand) is dependent on $\beta_{\theta_{\max}|S_a}$ which in turn tends to increase with ductility level.

4.15 Acknowledgements

The authors would like to acknowledge the Pacific Earthquake Engineering Research Center, PEER, funded by the U.S. National Science Foundation.